




Cite this: *J. Mater. Chem. C*, 2018, 6, 7549

Effect of a methyl thiophene-3-carboxylate bridge in an indacenodithiophene-based acceptor–donor–acceptor-type molecule on the performance of non-fullerene polymer solar cells†

Su Hong Park, Gi Eun Park, Suna Choi, Young Un Kim, Seo Yeon Park, Chang Geun Park, Min Ju Cho* and Dong Hoon Choi 

A new A-b-D-b-A-type n-type small molecule, **IDT-3MT**, was synthesized bearing a weak acceptor thiophene-3-carboxylate bridge (3MT = *b*) between indacenodithiophene as a donating core and 2-(3-oxo-2,3-dihydroinden-1-ylidene)-malononitrile as the accepting end groups. Compared to **IDT-T** bearing a neat thiophene bridge, **IDT-3MT** displayed a red-shifted absorption spectrum in the film state, which is a more effective complementary absorption behavior with PBDB-T as the donor material. The highest occupied molecular orbital and lowest unoccupied molecular orbital levels of **IDT-3MT** became correspondingly lower. Based on the results of grazing-incidence wide-angle X-ray scattering, the blend film of PBDB-T:**IDT-3MT** exhibited a more prominent face-on orientation and fine surface morphology compared with PBDB-T:**IDT-T**, which can facilitate charge transportation in the vertical direction. Among the two acceptors, the polymer solar cell based on a solvent additive-free as-cast PBDB-T:**IDT-3MT** blend film exhibited the highest power conversion efficiency of 8.40% with a high open-circuit voltage of 0.95 V and a short-circuit current density of 14.43 mA cm⁻² due to the more prominent face-on orientation and favorable morphology of the blend film. According to the simple structural modification of the acceptor molecule, the ester group in the thiophene bridge played an important role toward achieving high-performance polymer solar cells.

Received 31st March 2018,
Accepted 20th June 2018

DOI: 10.1039/c8tc01508b

rsc.li/materials-c

1. Introduction

Polymer solar cells (PSCs) with bulk heterojunction (BHJ)^{1,2} structures fabricated by simple solution-processing techniques are a cost-effective future alternative for utilizing solar energy and have advantages such as a light weight, processability, a variety of applied materials and device flexibility.^{3–6}

PSCs are typically fabricated by using a blend film consisting of conjugated polymer donors and small molecules, such as fullerene derivatives and acceptor–donor–acceptor (A–D–A)-type small molecules. Recently, many researchers have preferred A–D–A-type acceptors over fullerene derivatives due to the high tunability of their molecular structure and energy levels and broad absorption region from the visible to the near-infrared (NIR).^{7–10}

In order to develop high-performance A–D–A-type acceptors, 2-(3-oxo-2,3-dihydroinden-1-ylidene)-malononitrile (IC) as the accepting end-group and highly planar fused aromatic rings as the donating cores have been widely employed because they facilitate π -electron delocalization and improve the charge transport properties of the whole acceptor molecule.^{11–13} Among many A–D–A-type acceptors, IDT-IC, consisting of IC and indaceno[2,1-*b*:6,5-*b'*]dithiophene (IDT), has been proposed owing to its relatively low cost, simple synthesis procedures, high molar-extinction coefficients, NIR absorption region, and low-lying energy levels.^{2,13–18} Although IDT-IC has many advantages, as mentioned above, IDT-IC-based PSCs exhibited relatively poor device performance due to absorption spectral overlap with that of the donor polymer and highly crystalline behavior in the polymer blend film.¹⁴ For this reason, a few researchers have developed the molecular structure of IDT-IC by adding various conjugated bridges between IDT and ICs.

For example, Zhan *et al.* synthesized DC-IDT2T bearing thiophene bridges, and the corresponding PSCs showed a power conversion efficiency (PCE) of 3.93%, which was not significantly increased. Hou *et al.* demonstrated an IEICO acceptor with 3-((2-ethylhexyl)oxy)thiophene bridges.¹⁹ The PSCs based on IEICO

Department of Chemistry, Research Institute for Natural Sciences, Korea University, 145 Anam-ro, Sungbuk-gu, Seoul 02841, Republic of Korea.

E-mail: chominju@korea.ac.kr, dhchoi8803@korea.ac.kr;

Fax: +82 2 3290 3121; Tel: +82 2 3290 3140

† Electronic supplementary information (ESI) available: DFT calculation, UV, device structure, SCLC, GIWAXS and photovoltaic properties based on n-type small molecules. See DOI: 10.1039/c8tc01508b

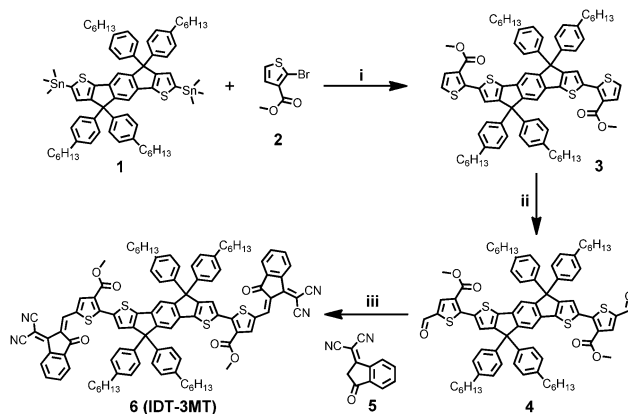
exhibited a highly improved PCE of 8.4% compared with the IEIC (4.9%) acceptor bearing 3-(2-ethylhexyl)thiophene bridges, and the IEICO based PSCs displayed a much wider photoresponse spectrum ($\sim 300\text{--}900\text{ nm}$) with a higher external quantum efficiency (EQE) value of 66% at 810 nm compared with that of the IEIC-based PSCs. The introduction of an alkoxy group to the thiophene bridge is an effective way to provide a low bandgap acceptor without reducing the open-circuit voltage (V_{OC}) of the PSCs. More recently, introducing noncovalent intramolecular interactions, well-known as “noncovalent conformational locking”, has become a widely adopted strategy for designing highly planar π -conjugated molecular systems for high performance organic electronics.²⁰ Huang *et al.* demonstrated a small molecular acceptor (IDT-Tz) using a relatively strong electron-withdrawing moiety of a thiazole bridge.²¹ The nitrogen atom of the thiazole unit and the sulfur atom of the IDT core may form sulfur–nitrogen ($\text{S} \cdots \text{N}$) noncovalent conformational locks to promote the stiffness and planarity of the backbone. IDT-Tz showed a lower the whole acceptor molecules LUMO level due to the electron-withdrawing thiazole bridges, which induced effective exciton dissociation. As a result, the PTB7-Th:IDT-Tz-blend-based PSCs exhibited a high PCE of 8.4%. Therefore, it is worthwhile introducing new conjugated bridges with noncovalent interactions and electron-withdrawing properties.

In this work, we demonstrated a new IDT-based small molecular acceptor, **IDT-3MT**, bearing weakly accepting methyl-3-thiophene-carboxylate groups between the IDT core and IC end-groups as a π -bridge to replace the neat electron-donating thiophene bridge in **IDT-T**. Compared to **IDT-T**, **IDT-3MT** showed somewhat low-lying energy levels and a red-shifted absorption spectrum in the film state. This means that 3MT as a weak accepting unit could change the energy levels and oxygen atoms in the ester unit and the sulfur atom in the IDT unit could induce planarity by forming oxygen–sulfur ($\text{S} \cdots \text{O}$) noncovalent conformational locks. Moreover, the polar ester groups in 3MT could induce a more obvious face-on orientation of the **IDT-3MT**-based blend film on the substrate. Solution-processed BHJ PSCs based on an as-cast PBDB-T:**IDT-3MT** blend film showed a PCE as high as 8.40%, which is much higher than that of the PBDB-T:**IDT-T**-based device (PCE = 6.36%) due to the more pronounced face-on orientation of polymer chains and favorable morphology of the blend film. The higher performance of PSCs fabricated using **IDT-3MT** and PBDB-T can be attributed to non-covalent interactions, which is similar to the excellent performance of PSCs using IEICO reported in the literature.¹⁹ It was clearly demonstrated that the addition of simple ester units to the thiophene bridge between the donor core and acceptor terminals could be very useful to realize highly efficient PSCs.

2. Results and discussion

2.1. Material synthesis and characterization

The synthetic route to a new indaceno[2,1-*b*:6,5-*b'*]dithiophene (IDT)-based acceptor, **IDT-3MT** (Scheme 1), displayed that the compound was prepared through a three-step synthesis. First, compound **3** was prepared in a yield of 79% by the Stille



Scheme 1 Synthetic procedures for intermediates and **IDT-3MT**. (i) $\text{Pd}_2(\text{dba})_3$, $\text{P}(\text{o-tolyl})_3$, toluene, N_2 , $90\text{ }^\circ\text{C}$, 16 h; (ii) LDA, THF, N_2 , $-78\text{ }^\circ\text{C}$, 1 h, then DMF, $-78\text{ }^\circ\text{C}$ to room temperature, 2 h; (iii) pyridine, chloroform (CHCl_3), N_2 , $65\text{ }^\circ\text{C}$, overnight.

coupling reaction between (4,4,9,9-tetrakis(4-hexylphenyl)-4,9-dihydro-s-indaceno[1,2-*b*:5,6-*b'*]dithiophene-2,7-diyl)bis(trimethyl stannane) (**1**)²² and methyl 2-bromothiophene-3-carboxylate (**2**).²³ Subsequently, compound **3** was treated with lithium diisopropylamide (LDA) at $-78\text{ }^\circ\text{C}$, followed by the addition of DMF, which yielded the formylated compound **4**. Compound **4** was reacted with 2-(3-oxo-2,3-dihydroinden-1-ylidene)malononitrile (**5**) via the Knoevenagel condensation reaction, which could provide the target molecule, **IDT-3MT**, in a yield of 82%.

Moreover, the small acceptor molecule **IDT-T** bearing the neat thiophene bridge was also synthesized as a control acceptor according to the reported literature.²⁴ **IDT-3MT** is highly soluble in common solvents, such as dichloromethane, chloroform, and chlorobenzene, at room temperature. The new compounds shown in the synthetic procedure were all characterized using $^1\text{H-NMR}$, $^{13}\text{C-NMR}$, MALDI-TOF, and elemental analysis.

2.2. Theoretical calculation

In order to investigate the optimized chemical geometries and molecular frontier orbitals of the two acceptor molecules **IDT-T** and **IDT-3MT**, density functional theory (DFT) calculations were carried out at the B3LYP/6-31G(d,p) level for investigating the structures with simplified side chains. As shown in Fig. 1, both the simplified small molecules **IDT-T** and **IDT-3MT** displayed highly planar conformations. The dihedral angle between the thiophene and the core unit was found to be 3.78° for **IDT-T** and 15.09° for **IDT-3MT** obtained by DFT calculation. In the case of **IDT-3MT**, the bulkier ester group is present in the side chain, and a much larger dihedral angle is predicted than in the case of **IDT-T**. However, it has been found that the planarity of the molecular structure is driven by the $\text{S} \cdots \text{O}$ noncovalent bond interaction.²⁰ The highest occupied molecular orbital (HOMO) of **IDT-T** was mainly distributed on the core, thiophene, and linked double bond, whereas the lowest unoccupied molecular orbital (LUMO) was delocalized along the backbone, as shown in Fig. S1 (ESI[†]). **IDT-3MT** also exhibits similar delocalized distributions of the HOMO and LUMO. In general, the coplanar

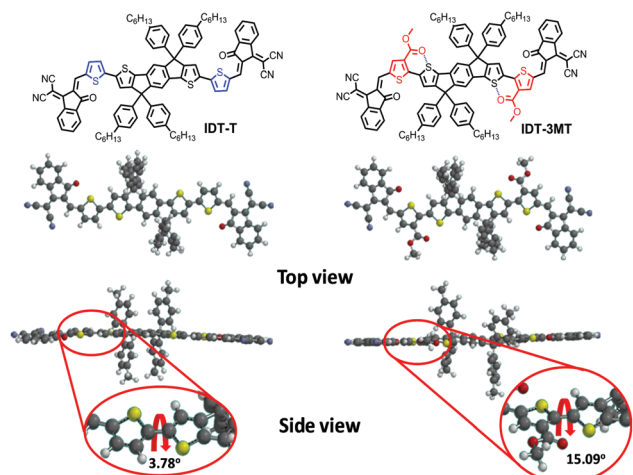


Fig. 1 Theoretically calculated optimized geometries of **IDT-T** and **IDT-3MT** using DFT calculations. The alkyl chains are replaced with methyl groups for computational simplicity.

structure of the conjugated fused-core moieties promotes intermolecular π - π stacking. Compared to **IDT-T** with thiophene as a π -bridge, the 3MT unit can be expected to enhance the stiffness of the backbone of **IDT-3MT** through an extraordinary secondary interaction between the sulfur and oxygen atoms.

2.3. Optical and electrochemical properties

To investigate the optical properties of the small molecular acceptors, UV-visible (UV-vis) absorption spectra were recorded. The UV-vis absorption spectra of **IDT-T** and **IDT-3MT** in chloroform solutions and thin solid films are shown in Fig. 2a and b, respectively. The detailed spectroscopic data are summarized in Table 1. In the chloroform (CHCl_3) solution, the main absorption band of **IDT-3MT** extends from 550 nm to 780 nm with a maximum absorption peak ($\lambda_{\text{max}}^{\text{abs}}$) at 683 nm, which is blue-shifted by ~ 15 nm relative to that of **IDT-T**. **IDT-3MT** in chloroform (concentration 10^{-6} M) exhibits strong absorption in the region of 500–750 nm with a maximum extinction coefficient (ϵ) of $1.33 \times 10^5 \text{ M}^{-1} \text{ cm}^{-1}$ at 683 nm, which is slightly higher than that of **IDT-T** in chloroform ($1.19 \times 10^5 \text{ M}^{-1} \text{ cm}^{-1}$ at 698 nm) (Fig. S2, ESI †). Compared to the solutions, the absorption spectrum of the **IDT-3MT** film exhibited a red shift of ~ 38 nm, with an absorption edge ($\lambda_{\text{cut-off}}^{\text{abs}}$) appearing at 812 nm. The optical bandgap ($E_{\text{g}}^{\text{opt}}$) of 1.52 eV is 0.04 eV smaller than that of **IDT-T** ($E_{\text{g}}^{\text{opt}} = 1.56$ eV). It is expected that the **IDT-3MT**-based blend film with donor polymer PBDB-T would show broader complementary absorption behavior. Cyclic voltammetry (CV) was used to investigate the energy levels electrochemically (Fig. 2c and d). The HOMO and LUMO levels of **IDT-3MT** were calculated as -5.68 and -4.16 eV, respectively, from the onset of the oxidation and reduction potentials,

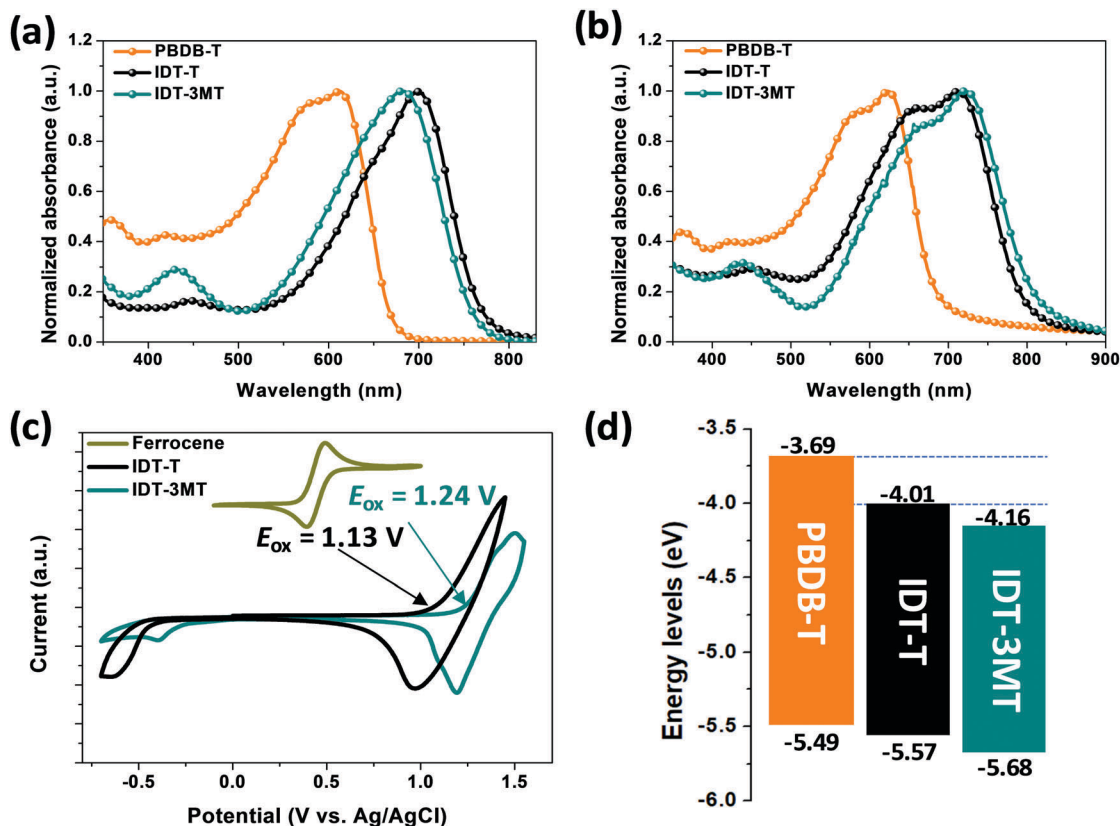


Fig. 2 Normalized absorption spectra of PBDB-T as the donor polymer and **IDT-T** and **IDT-3MT** as small acceptor molecules in (a) solution and (b) films. (c) Cyclic voltammograms of the two small molecules in the films. (d) Energy level alignment observed in PBDB-T as a donor with **IDT-T** and **IDT-3MT** as the acceptors used in this study.

Table 1 Optical and electrochemical properties of IDT-T and IDT-3MT

Acceptor	Absorption (nm)		ϵ_{max}^a ($\text{M}^{-1} \text{cm}^{-1}$)	$\lambda_{\text{cut-off}}^b$ (nm)	$E_g^{\text{opt}c}$ (eV)	E_{ox}^d (V)	Energy levels (eV)	
	Solution	Film					HOMO ^d	LUMO ^e
IDT-T	698	711	1.19×10^5	795	1.56	1.13	−5.57	−4.01
IDT-3MT	683	721	1.33×10^5	812	1.52	1.24	−5.68	−4.16

^a Chloroform solution. ^b Thin film. ^c The optical bandgaps were obtained from absorption spectra of film samples ($E_g^{\text{opt}} = 1240/\lambda_{\text{cut-off}}$). ^d Obtained from cyclic voltammograms of films on Pt electrodes. ^e $E_{\text{LUMO}} = E_{\text{HOMO}} + E_g^{\text{opt}}$.

according to $E_{\text{HOMO/LUMO}} = -e(E_{\text{ox/red}} + 4.80)$ (eV). For IDT-T, the HOMO and LUMO are located at −5.57 and −4.01 eV, respectively. In comparison with IDT-T, both the HOMO and LUMO energy levels of IDT-3MT were decreased by 0.11 eV and 0.15 eV, respectively, which is consistent with the effect of the weak electron-withdrawing properties of the 3MT unit. In brief, owing to the electron-withdrawing characteristic of 3MT, IDT-3MT exhibited lower-lying HOMO and LUMO levels. The absorption spectrum of the IDT-3MT film was observed to be red-shifted compared to that of IDT-T film, suggesting that π - π interactions were highly promoted in the solid state.²⁵ This is mainly attributed to the interaction between the sulfur and oxygen atoms, which yields a more coplanar structure. The absorption spectra in solutions and CV measurements clearly demonstrated that the introduction of the ester moiety in the thiophene bridge slightly decreased the HOMO and LUMO energy levels and the optical bandgap (E_g^{opt}).

2.4. Photovoltaic properties of IDT-3MT-based PSCs

To assess the photovoltaic properties of IDT-3MT, we fabricated a PSC device with a configuration of indium tin oxide (ITO)/zinc oxide (ZnO)/active layer/molybdenum(vi) oxide (MoO_3)/silver (Ag) as an inverted structure, where ZnO and MoO_3 were used as the electron-transport and hole-transport layers, respectively (Fig. S3, ESI†). To attempt effective comparisons, PSCs based on PBDB-T:IDT-T blends were also prepared under the same conditions and device configuration.

PSC devices were fabricated by varying the blend ratio of the donor polymer, PBDB-T, and the two acceptors, as well as the active layer thickness (~ 90 nm) to optimize the fabrication conditions. It was found that a 1:1 (w/w) blend ratio of donor polymer and acceptor in chlorobenzene provided the best photovoltaic performance (Fig. S4, ESI†). The detailed device performance data are summarized in Tables S1 and S2 (ESI†). As shown in Fig. 3a, the current density versus voltage (J - V) curves,

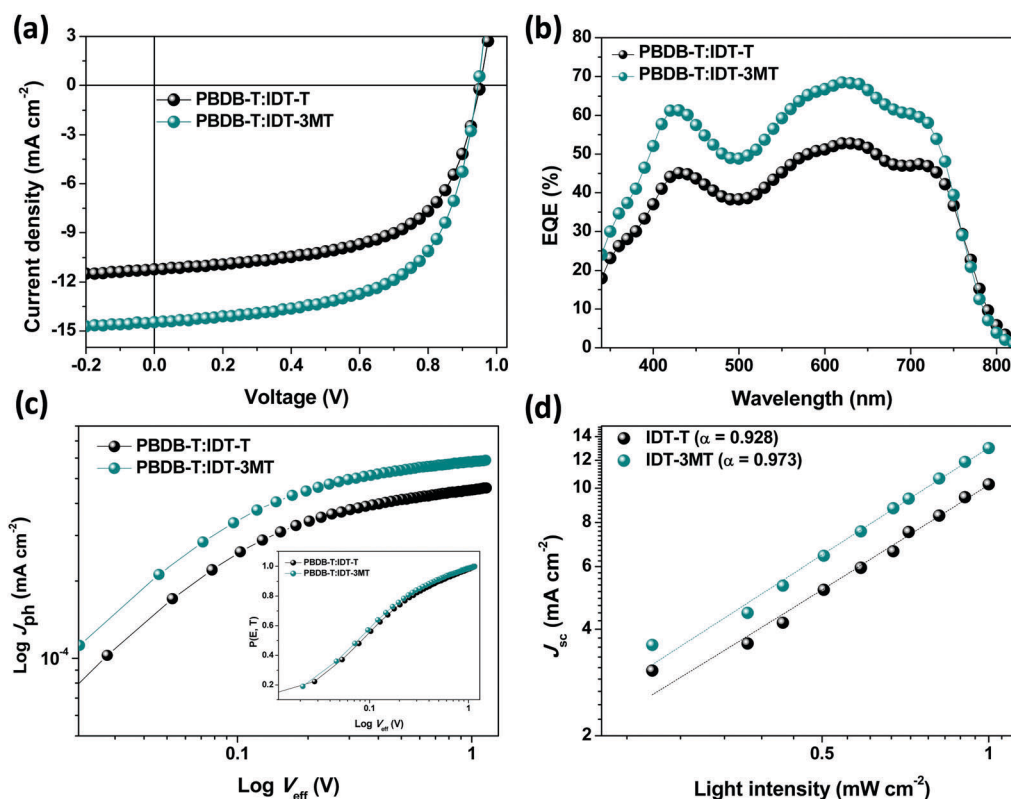


Fig. 3 (a) J - V characteristics and (b) EQE spectra of PSCs with photoactive layers of PBDB-T:IDT-T and PBDB-T:IDT-3MT. (c) Photocurrent density versus effective voltage characteristics (inset: plots of $J_{\text{ph}}/J_{\text{sat}}$ versus effective voltage). (d) Plots of short-circuit current versus light intensity.

Table 2 Photovoltaic performance of PSCs with a device structure of ITO/ZnO/PBDB-T:acceptors (1:1, w/w)/MoO₃/Ag under AM 1.5G illumination (100 mW cm⁻²)

Acceptor	V_{OC} (V)	J_{SC} (mA cm ⁻²)	FF (%)	PCE (%)	μ_h (cm ² V ⁻¹ s ⁻¹)	μ_e (cm ² V ⁻¹ s ⁻¹)	μ_h/μ_e
IDT-T	0.952 (0.950 ± 0.008)	11.21 (10.96 ± 0.15)	59.62 (60.24 ± 1.11)	6.36 (6.28 ± 0.15)	1.66×10^{-4}	8.19×10^{-6}	20.27
IDT-3MT	0.950 (0.946 ± 0.005)	14.43 (13.78 ± 0.48)	61.32 (61.43 ± 0.62)	8.40 (7.96 ± 0.36)	2.07×10^{-5}	1.02×10^{-5}	2.03

Average values with standard deviations were obtained from more than 10 devices.

and the corresponding photovoltaic parameters in Table 2, the blend film with a 1:1 wt ratio of donor polymer (PBDB-T) and acceptor molecule showed the best performance in terms of PCE: the PBDB-T:**IDT-3MT** device revealed a PCE of 8.40% with a high short-circuit current density (J_{SC}) of 14.43 mA cm⁻², open-circuit voltage (V_{OC}) of 0.95 V, and fill factor (FF) of 61.32%, and the corresponding energy loss was as low as 0.570 eV. In contrast, the PBDB-T:**IDT-T** device showed a J_{SC} of 11.21 mA cm⁻², V_{OC} of 0.952 V, and a FF of 59.62%, resulting in a PCE of 6.36%, and the corresponding energy loss was 0.608 eV. The photon energy loss (E_{loss}) was calculated using the formula $E_{loss} = E_g - eV_{OC}$.^{26,27} Compared with **IDT-T**, the **IDT-3MT**-based devices exhibit a slightly lower V_{OC} but much higher J_{SC} and FF; the lower V_{OC} is mainly due to the slightly deeper LUMO of **IDT-3MT**, and the higher J_{SC} may be due, in part, to a larger LUMO energy difference (ΔE_{LUMO}) between PBDB-T and **IDT-3MT**, leading to more efficient exciton dissociation.⁴ Moreover, the improved FF can be attributed to the highly planar acceptor structures and J_{SC} . It is conjectured that the enhancement factor of FF is probably due to the efficient charge separation from loosely bound holes and electrons in the charge-transfer state with a smaller degree of bimolecular recombination. External quantum efficiency (EQE) measurements were carried out and the EQE spectra are illustrated in Fig. 3b. The PBDB-T:**IDT-3MT** device displayed a broad spectral response in the region 340–850 nm, and the PBDB-T:**IDT-T** device showed a similar light-harvesting phenomenon. The EQE values of PBDB-T:**IDT-3MT** were higher than those of PBDB-T:**IDT-T** across the whole spectrum, reaching a maximum EQE value of 68.5% at 620 nm. To investigate the charge generation, dissociation, and extraction properties, we measured the dependence of photocurrent density (J_{ph}) on the effective voltage (V_{eff}) of the device (Fig. 3c). J_{ph} can be defined as $J_{ph} = J_L - J_D$, where J_L and J_D are the current densities under illumination and in the dark, respectively. V_{eff} can be defined as $V_{eff} = V_0 - V_{bias}$, where V_0 is the voltage at which the photocurrent is zero and V_{bias} is the applied external voltage bias.^{28,29} J_{sat} of the **IDT-3MT**-based PSCs is 14.76 mA cm⁻², which is higher than that of the **IDT-T**-based PSCs (11.49 mA cm⁻²), which is partially due to better light harvesting and a higher degree of exciton generation. As shown in the inset of Fig. 3c, under short-circuit conditions, an exciton dissociation probability ($P(E,T) = J_{ph}/J_{sat}$, where J_{sat} is the saturation photocurrent density) of 98.2% was obtained for the PBDB-T:**IDT-3MT**-based device. In contrast, the $P(E,T)$ value of the PBDB-T:**IDT-T**-based devices was 97.6%, indicating that both devices have excellent exciton dissociation and charge collection efficiency, although the $P(E,T)$ value of the PBDB-T:**IDT-3MT**-based device was slightly higher. We also measured J_{SC} versus light intensity (P_{light}) to study the charge-recombination behavior (Fig. 3d). The relationship

between J_{SC} and P_{light} can be described as $J_{SC} \propto P_{light}^{\alpha}$.^{28–30} When all the charges are collected by the electrode before recombination, α should be equal to 1, and $\alpha < 1$ means that charge recombination occurs to some extent. The α value of the **IDT-3MT**-based PSC is 0.973, indicating that the molecular recombination is effectively reduced, whereas the **IDT-T**-based device exhibits a slightly higher degree of bimolecular recombination with an α value of 0.928.

2.5. Charge-carrier mobility in blend films

To understand the influence of the charge transport capability on photovoltaic performance, the hole and electron mobilities of the blend films were measured using the space-charge-limited current (SCLC) method with the device structures of ITO/poly(3,4-ethylenedioxythiophene):polystyrene sulfonate (PEDOT:PSS)/active layer/Au for a hole-only device and ITO/ZnO/active layer/LiF/Al for an electron-only device, displayed in Fig. S5a and b (ESI[†]), respectively. The hole and electron carrier mobilities were calculated by fitting the measured J - V curve in the near-quadratic region using a well-known modified Mott-Gurney equation.³¹ The electron mobilities of the **IDT-T** and **IDT-3MT**-based devices in blended films are 8.19×10^{-6} and 1.02×10^{-5} cm² V⁻¹ s⁻¹, respectively, and the hole mobilities of the **IDT-T** and **IDT-3MT** blended films are 1.66×10^{-4} and 2.07×10^{-5} cm² V⁻¹ s⁻¹, respectively. The μ_h/μ_e values of the **IDT-T** and **IDT-3MT**-based devices are 20.27 and 2.03, respectively (Table 2). Although the values of the mobility of holes in the PBDB-T:**IDT-T** blended film are relatively higher, the more balanced charge transport in the PBDB-T:**IDT-3MT** blended film is responsible for the higher J_{SC} and FF of the corresponding PSC.

2.6. Photoinduced PL-quenching behavior in blend films

As shown in Fig. 4, a photoluminescence (PL)-quenching experiment was performed to verify the exciton dissociation and charge-transfer behavior in the blend films, where the excitation wavelengths of 600 nm for PBDB-T and 700 nm for **IDT-T** and **IDT-3MT** as the acceptor were selected according to their maximum absorption range. The PL spectra of the blend films were compared with those of pristine donor or acceptor films. When excited at a wavelength of 600 nm, the PL emission peak of PBDB-T appears in the range 620–850 nm, centered at 685 nm. For the blend films, the emission of PBDB-T was quenched, suggesting efficient photoinduced electron transfer from the donor to acceptor for the excitons produced in the donor phase. For the **IDT-T** and **IDT-3MT** acceptors, their emissions were found in the range 750–900 nm when excited at a wavelength of 700 nm. Compared to the PBDB-T:**IDT-T** blend film, the PBDB-T:**IDT-3MT** blend film results in a fluorescence quenching efficiency of over 95% at a wavelength of 810 nm,

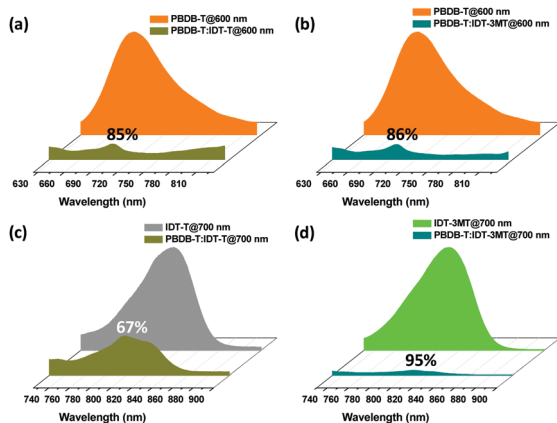


Fig. 4 PL spectra of (a and b) PBDB-T (excited at 600 nm), (c) IDT-T (excited at 700 nm), (d) IDT-3MT (excited at 700 nm), as well as blend films of PBDB-T:IDT-T (excited at (a) 600 nm and (c) 700 nm) and PBDB-T:IDT-3MT (excited at (b) 600 nm and (d) 700 nm).

which is more efficient than that of PBDB-T:IDT-T (67%). This observation suggested that the PBDB-T:IDT-3MT-blend film can exhibit more efficient exciton dissociation and charge transfer to produce a high J_{SC} in PSCs.

2.7. Morphological characteristics of the blend films

To find more evidence of the PSC performance, the surface and internal morphologies of the optimized blend films were investigated by atomic force microscopy (AFM) and transmission electron microscopy (TEM), respectively. The height and phase AFM images ($2 \mu\text{m} \times 2 \mu\text{m}$) of the blend films are shown in Fig. 5. The PBDB-T:IDT-T- and PBDB-T:IDT-3MT blend films exhibit uniform and smooth surfaces with relatively small root-mean-square (RMS) roughness values of less than 1.2 nm. For the PBDB-T:IDT-T blend film (Fig. 5a and b), slightly larger surface aggregates were observed, and the RMS roughness R_q increased to 1.165 nm. The RMS roughness of the PBDB-T:IDT-3MT film was lower than 0.7 nm, which suggests that the IDT-3MT molecules reached a higher degree of mixing with PBDB-T in the blend films

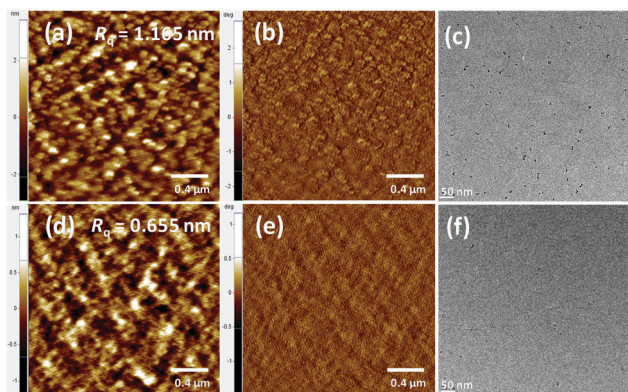


Fig. 5 AFM (a and d) height images and (b and e) phase images ($2 \mu\text{m} \times 2 \mu\text{m}$) of the optimized PBDB-T-acceptor blend films (1:1 w/w) prepared in chlorobenzene. (a and b) PBDB-T:IDT-T and (d and e) PBDB-T:IDT-3MT. TEM images of (c) PBDB-T:IDT-T and (f) PBDB-T:IDT-3MT.

(Fig. 5d and e). In order to investigate the effect of the solvent additive, we compared the surface morphology of the PBDB-T:IDT-3MT active layer of the device without and with additive (Fig. S6, ESI†). A smooth and uniform surface was observed in the active layer without additive. However, the R_q of the active layer surface increased and the domain size became larger after addition of DIO than that of the active layer without DIO. As a result, the J_{SC} value of the PSC with the active layer with DIO was reduced, resulting in adverse effects on exciton diffusion, dissociation and charge transport. Eventually, the PCE of the PSC also decreased. (Table S1, ESI†).

TEM was used to investigate the internal morphology of the active layer in the PSCs. The PBDB-T:IDT-3MT blend film (Fig. 5f) showed nanophase segregation in the blend film compared to the PBDB-T:IDT-T blend film, which showed a high extent of self-assembling behavior to produce larger agglomerates (Fig. 5c). This is an adverse obstacle to exciton diffusion and has a negative effect of increasing the probability of charge recombination in the associated PSC device. Advantageous nanoscale phase separation characteristics in the active layer based on IDT-3MT facilitated the charge generation and transport processes in the PSCs, resulting in a high J_{SC} value.

Fig. 6 exhibits the grazing-incidence wide-angle X-ray diffraction (GIWAXD)³² patterns of both acceptor films and PBDB-T-based blend films with the corresponding out-of-plane and in-plane line profiles. Table S3 (ESI†) lists the diffraction parameters of PBDB-T, IDT-T and IDT-3MT in the pristine films and blend films with acceptors obtained from the GIWAXD measurements. For the IDT-T and IDT-3MT pristine films, the sharp peaks at $q_{xy} \approx 0.32$ and 0.33 \AA^{-1} originate from lamellar packing in the in-plane profiles of IDT-T ($d_{(100)} = 19.47 \text{ \AA}$) and IDT-3MT ($d_{(100)} = 19.30 \text{ \AA}$), respectively. Pristine films of IDT-T and IDT-3MT showed obvious crystalline properties with a strong (010) π - π stacking peak in the out-of-plane direction, which means a typical face-on orientation with a π - π stacking peak located at 1.76 \AA^{-1} ($d_{(010)} \approx 3.52 \text{ \AA}$). As shown in Fig. 6(f), the PBDB-T pristine film shows a pronounced lamellar packing (100) diffraction peak ($q_{xy} \approx 0.29 \text{ \AA}^{-1}$, $d_{(100)} = 21.78 \text{ \AA}$) in the in-plane direction. A (010) π - π stacking peak at $q_z \approx 1.67 \text{ \AA}^{-1}$ ($d_{(010)} = 3.73 \text{ \AA}$) and a (100)

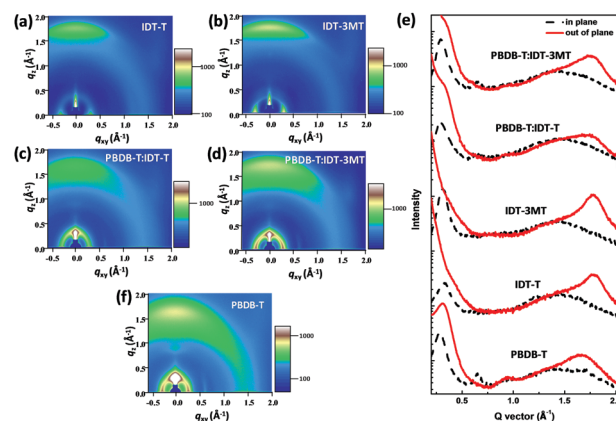


Fig. 6 2D GIWAXD patterns for pristine films of (a) IDT-T, (b) IDT-3MT, (f) PBDB-T, and blend films of (c) PBDB-T:IDT-T and (d) PBDB-T:IDT-3MT. (e) In-plane and out-of-plane scattering profiles of the GIWAXD patterns.

diffraction peak at $q_z \approx 0.29 \text{ \AA}^{-1}$ ($d_{(010)} = 21.78 \text{ \AA}$) can be clearly seen in the out-of-plane direction. These results suggest that the face-on chain orientation of PBDB-T is relatively dominant. According to Table S3 (ESI[†]), the (100) lamellar stacking and (010) π - π stacking peaks observed in the diffraction profiles of blend films were found to originate from the crystalline donor polymer and acceptor domains, respectively. In the out-of-plane profile of PBDB-T:IDT-3MT, the (010) diffraction peak ($d_{(010)} = 3.50 \text{ \AA}$) was more sharp and stronger than that of PBDB-T:IDT-T. It is believed that the crystallization of IDT-3MT acceptor molecules is enhanced irrespective of bulky ester substituents, and that the ordered structure is favourable in a face-on mode. This might be attributed to the strong intermolecular interaction of IDT-3MT through intramolecular S \cdots O interactions, resulting in the dense packing of these molecules.

3. Conclusions

A new IDT-based A-b-D-b-A-type acceptor, IDT-3MT, bearing 3MT(=b) bridges between IDT and ICs, was successfully synthesized. IDT-3MT showed relatively low-lying energy levels and a red-shifted absorption spectrum compared to IDT-T bearing thiophene bridges. The BHJ PSC based on the as-cast PBDB-T:IDT-3MT blend film exhibited the highest PCE of 8.4% with a high V_{OC} of 0.95 V and J_{SC} of 14.43 mA cm^{-2} due to the more prominent face-on orientation and fine internal morphology of the blend film. With the simple structural modification of the acceptor molecule, the ester group in the 3MT structure played an important role in conferring advantages to the high-performance PSCs without requiring a complicated synthesis and design strategy.

4. Experimental section

4.1. Materials

All the chemicals were purchased from Sigma-Aldrich or Acros Organics and used without further purification. 2,2'-((2Z,2'-Z)-((5,5'-(4,4,9,9-Tetrakis(4-hexylphenyl)-4,9-dihydro-s-indaceno[1,2-b:5,6-b']dithiophene-2,7-diyl)bis(thiophene-5,2-diyl))bis(methanylylidene))bis(3-oxo-2,3-dihydro-1H-indene-2,1-diylidene))dimalononitrile (IDT-T), and compounds 1 and 2 were synthesized according to reported literature procedures.^{21–23}

4.1.1. Synthesis of dimethyl 2,2'-(4,4,9,9-tetrakis(4-hexylphenyl)-4,9-dihydro-s-indaceno[1,2-b:5,6-b']dithiophene-2,7-diyl)-bis(thiophene-3-carboxylate) (compound 3). Compound 3 was synthesized by the conventional Stille coupling reaction. Compound 1 (0.84 g, 0.68 mmol) and compound 2 (300 mg, 1.36 mmol) were added into a 50 mL two-neck flask, and 10 mL of toluene and 1 mL of DMF were added. The mixture was purged with N_2 for 5 min, and then 25 mg of catalyst ($Pd_2(dba)_3$) and $P(o\text{-tolyl})_3$ were added. After being purged for another 15 min with N_2 , the reaction was moved to a 110°C oil bath and stirred for 3 h. The solvent was then removed by rotary evaporation, and the crude product was purified by silica-gel column chromatography. The pure compound 3 was obtained as an orange solid (637 mg, yield 79%). $^1\text{H-NMR}$ (500 MHz, $CDCl_3$): δ (ppm) 7.45 (s, 2H), 7.44 (d, $J = 5.5 \text{ Hz}$, 2H),

7.35 (s, 2H), 7.17 (d, $J = 8 \text{ Hz}$, 8H), 7.12 (d, $J = 5.5 \text{ Hz}$, 2H), 7.06 (d, $J = 8 \text{ Hz}$, 8H), 3.77 (s, 6H), 2.56 (m, 8H), 1.58 (m, 8H), 1.31 (m, 24H), 0.87 (m, 12H). $^{13}\text{C-NMR}$ (125 MHz, $CDCl_3$): δ (ppm) 163.75, 155.59, 153.35, 144.09, 143.77, 141.70, 141.54, 136.08, 135.32, 130.64, 128.37, 127.87, 126.76, 125.23, 123.40, 117.77, 63.03, 51.72, 35.57, 31.73, 31.37, 29.14, 22.60, 14.12. MS (MALDI-TOF): m/z 1186.41 (M^+). Anal. calc. for $C_{76}H_{82}O_4S_4$: C, 76.85; H, 6.96; O, 5.39; S, 10.80.

4.1.2. Synthesis of dimethyl 2,2'-(4,4,9,9-tetrakis(4-hexylphenyl)-4,9-dihydro-s-indaceno[1,2-b:5,6-b']dithiophene-2,7-diyl)-bis(5-formylthiophene-3-carboxylate) (compound 4). LDA (2 M, 5 mL) was added dropwise to the solution of compound 3 (2.32 g, 1.95 mmol) in anhydrous THF (25 mL) at -78°C under an N_2 atmosphere. The mixture was stirred for 1 h at low temperature, and DMF (2.28 g, 31.19 mmol) was added in one portion. After 10 min, the low-temperature bath was removed and the reaction mixture was stirred at room temperature for 2 h. Subsequently, the mixture was quenched using water and extracted three times by MC. After the combined organic phase was concentrated, further purification was carried out by silica-gel column chromatography to produce pure compound 4, which was obtained as a dark orange solid (1.82 g, yield 75%). $^1\text{H-NMR}$ (500 MHz, $CDCl_3$): δ (ppm) 9.82 (s, 2H), 8.10 (s, 2H), 7.60 (s, 2H), 7.50 (s, 2H), 7.15 (d, $J = 8 \text{ Hz}$, 8H), 7.08 (d, $J = 8 \text{ Hz}$, 8H), 3.84 (s, 6H), 2.56 (m, 8H), 1.61 (m, 8H), 1.30 (m, 24H), 0.87 (m, 12H). $^{13}\text{C-NMR}$ (125 MHz, $CDCl_3$): δ (ppm) 182.25, 162.91, 156.38, 154.00, 152.25, 146.61, 141.86, 141.18, 139.77, 139.06, 135.51, 135.39, 128.52, 127.76, 127.14, 126.55, 118.30, 63.09, 52.17, 35.57, 31.72, 31.35, 29.12, 22.60, 14.12. MS (MALDI-TOF): m/z 1242.32 (M^+). Anal. calc. for $C_{78}H_{82}O_6S_4$: C, 75.32; H, 6.65; O, 7.72; S, 10.31.

4.1.3. Synthesis of IDT-3MT (compound 6). To a mixture of compound 4 (138 mg, 0.11 mmol) and 2-(3-oxo-2,3-dihydro-1H-inden-1-ylidene)malononitrile (194 mg, 1 mmol) in 30 mL of chloroform, pyridine (0.3 mL) was added at room temperature. After 0.5 h of stirring at room temperature, the mixture was placed in an oil bath at 65°C and stirred for another 24 h. The mixture was precipitated in ethanol and filtered through a Buchner funnel, and the solid was washed by methanol. The product of IDT-3MT (158 mg, yield 89%) was purified by silica-gel column chromatography using dichloromethane as the eluent. $^1\text{H-NMR}$ (500 MHz, $CDCl_3$): δ (ppm) 8.76 (s, 2H), 8.71 (dd, $J = 8 \text{ Hz}$, 2H), 8.16 (s, 2H), 7.94 (dd, $J = 8 \text{ Hz}$, 2H), 7.82 (s, 2H), 7.79 (m, 4H), 7.53 (s, 2H), 7.19 (d, $J = 8 \text{ Hz}$, 8H), 7.10 (d, $J = 8 \text{ Hz}$, 8H), 3.90 (s, 6H), 2.58 (m, 8H), 1.61 (m, 8H), 1.30 (m, 24H), 0.87 (m, 12H). $^{13}\text{C-NMR}$ (125 MHz, $CDCl_3$): δ (ppm) 188.51, 162.89, 159.69, 157.02, 156.29, 154.58, 148.62, 148.49, 141.90, 141.02, 140.07, 137.20, 136.92, 136.70, 135.99, 135.77, 135.57, 134.78, 132.78, 128.60, 127.83, 127.60, 126.45, 125.46, 123.99, 123.63, 118.52, 114.18, 70.63, 63.16, 52.34, 35.59, 31.73, 31.37, 29.13, 22.60, 14.12. MS (MALDI-TOF): m/z 1595.58 (M^+). Anal. calc. for $C_{102}H_{90}N_4O_6S_4$: C, 76.76; H, 5.68; N, 3.51; O, 6.01; S, 8.04.

Conflicts of interest

There are no conflicts to declare.

Acknowledgements

This work was supported by the National Research Foundation of Korea (NRF2015R1A2A1A05001876) and by the Key Research Institute Program (NRF20100020209).

Notes and references

- 1 Y. Lin, F. Zhao, Y. Wu, K. Chen, Y. Xia, G. Li, S. K. Prasad, J. Zhu, L. Huo, H. Bin, Z. G. Zhang, X. Guo, M. Zhang, Y. Sun, F. Gao, Z. Wei, W. Ma, C. Wang, J. Hodgkiss, Z. Bo, O. Inganas, Y. Li and X. Zhan, *Adv. Mater.*, 2017, **29**, 1604155.
- 2 Y. Lin, J. Wang, Z. G. Zhang, H. Bai, Y. Li, D. Zhu and X. Zhan, *Adv. Mater.*, 2015, **27**, 1170–1174.
- 3 Y. J. Cheng, S. H. Yang and C. S. Hsu, *Chem. Rev.*, 2009, **109**, 5868–5923.
- 4 Y. Li, *Acc. Chem. Res.*, 2012, **45**, 723–733.
- 5 Y. Lin, Y. Li and X. Zhan, *Chem. Soc. Rev.*, 2012, **41**, 4245–4272.
- 6 G. Li, R. Zhu and Y. Yang, *Nat. Photonics*, 2012, **6**, 153–161.
- 7 Y. Lin and X. Zhan, *Mater. Horiz.*, 2014, **1**, 470–488.
- 8 C. Zhan, X. Zhang and J. Yao, *RSC Adv.*, 2015, **5**, 93002–93026.
- 9 W. Chenab and Q. Zhang, *J. Mater. Chem. C*, 2017, **5**, 1275–1302.
- 10 Z. Li, K. Jiang, G. Yang, J. Y. L. Lai, T. Ma, J. Zhao, W. Ma and H. Yan, *Nat. Commun.*, 2016, **7**, 13094.
- 11 C. B. Nielsen, S. Holliday, H. Chen, S. J. Cryer and I. McCulloch, *Acc. Chem. Res.*, 2015, **48**, 2803–2812.
- 12 Y. Lin and X. Zhan, *Acc. Chem. Res.*, 2016, **49**, 175–183.
- 13 Y. Lin, Z. G. Zhang, H. Bai, J. Wang, Y. Yao, Y. Li, D. Zhu and X. Zhan, *Energy Environ. Sci.*, 2015, **8**, 610–616.
- 14 Y. Lin, T. Li, F. Zhao, L. Han, Z. Wang, Y. Wu, Q. He, J. Wang, L. Huo, Y. Sun, C. Wang, W. Ma and X. Zhan, *Adv. Energy Mater.*, 2016, **6**, 1600854.
- 15 Y. Lin, F. Zhao, Q. He, L. Huo, Y. Wu, T. C. Parker, W. Ma, Y. Sun, C. Wang, D. Zhu, A. J. Heeger, S. R. Marder and X. Zhan, *J. Am. Chem. Soc.*, 2016, **138**, 4955–4961.
- 16 X. Guo, M. Zhang, J. Tan, S. Zhang, L. Huo, W. Hu, Y. Li and J. Hou, *Adv. Mater.*, 2012, **24**, 6536–6541.
- 17 Y. Zhang, J. Zou, H. L. Yip, K. S. Chen, D. F. Zeigler, Y. Sun and A. K. Y. Jen, *Chem. Mater.*, 2011, **23**, 2289–2291.
- 18 W. Zhang, J. Smith, S. E. Watkins, R. Gysel, M. McGehee, A. Salleo, J. Kirkpatrick, S. Ashraf, T. Anthopoulos, M. Heeney and I. McCulloch, *J. Am. Chem. Soc.*, 2010, **132**, 11437–11439.
- 19 H. Yao, Y. Chen, Y. Qin, R. Yu, Y. Cui, B. Yang, S. Li, K. Zhang and J. Hou, *Adv. Mater.*, 2016, **28**, 8283–8287.
- 20 Y. Liu, Z. Zhang, S. Feng, M. Li, L. Wu, R. Hou, X. Xu, X. Chen and Z. Bo, *J. Am. Chem. Soc.*, 2017, **139**, 3356–3359.
- 21 S. Yu, Y. Chen, L. Yang, P. Ye, J. Wu, J. Yu, S. Zhang, Y. Gao and H. Huang, *J. Mater. Chem. A*, 2017, **5**, 21674–21678.
- 22 Y. C. Chen, C. Y. Yu, Y. L. Fan, L. I. Hung, C. P. Chen and C. Ting, *Chem. Commun.*, 2010, **46**, 6503.
- 23 W. Zhang, J. Cao, Y. Liu, Z. Xiao, W. Zhu, Q. Zuo and L. Ding, *Macromol. Rapid Commun.*, 2012, **33**, 1574–1579.
- 24 H. Bai, Y. Wang, P. Cheng, J. Wang, Y. Wu, J. Hou and X. Zhan, *J. Mater. Chem. A*, 2015, **3**, 1910–1914.
- 25 S. Albrecht, J. R. Tumbleston, S. Janietz, I. Dumsch, S. Allard, U. Scherf, H. Ade and D. Neher, *J. Phys. Chem. Lett.*, 2014, **5**, 1131–1138.
- 26 D. Veldman, S. C. J. Meskers and R. A. J. Janssen, *Adv. Funct. Mater.*, 2009, **19**, 1939–1948.
- 27 K. Kawashima, Y. Tamai, H. Ohkita, I. Osaka and K. Takimiya, *Nat. Commun.*, 2015, **6**, 10085.
- 28 H. Lin, S. Chen, Z. Li, J. Y. Lai, G. Yang, T. McAfee, K. Jiang, Y. Li, Y. Liu, H. Hu, J. Zhao, W. Ma, H. Ade and H. Yan, *Adv. Mater.*, 2015, **27**, 7299–7304.
- 29 Q. H. Wu, D. L. Zhao, A. M. Schneider, W. Chen and L. P. Yu, *J. Am. Chem. Soc.*, 2016, **138**, 7248–7251.
- 30 L. Gao, Z. Zhang, H. Bin, L. Xue, Y. Yang, C. Wang, F. Liu, T. P. Russell and Y. Li, *Adv. Mater.*, 2016, **28**, 8288–8295.
- 31 Y. Shirota and H. Kageyama, *Chem. Rev.*, 2007, **107**, 953–1010.
- 32 A. Hexemer, W. Bras, J. Glossinger, E. Schaible, E. Gann, R. Kirian, A. MacDowell, M. Church, B. Rude and H. Padmore, *J. Phys.: Conf. Ser.*, 2010, **247**, 012007.